Turk J Elec Engin, VOL.16, NO.1 2008, © TÜBİTAK

Comparison of Rectangular and Cylindrical FDTD representations on a Ring Resonator Problem

Funda AKLEMAN[1], **Levent SEVGİ**[2]
[1]*İstanbul Technical University, Electronics and Communication Engineering Department, Maslak, 34469 İstanbul-TURKEY*
e-mail: akleman@itu.edu.tr
[2]*Doğuş University, Electronics and Communication Engineering Department, Zeamet Sok. No. 21, Acıbadem 34722 İstanbul-TURKEY*
e-mail: lsevgi@itu.edu.tr

Abstract

The aim of this paper is to discuss rectangular and cylindrical representations of finite-difference time-domain (FDTD) method over characteristic tests and comparisons. A ring resonator is chosen as a canonical structure and modeled with both rectangular- and cylindrical-FDTD packages. Calibration against analytical exact solution derived in terms of cylindrical Bessel functions is also performed. It is shown that rectangular-FDTD with periodic boundary condition, where the computation domain is reduced, can also be applied in modeling circular structures.

1. Introduction

A ring (circular) resonator with rectangular cross-section and perfectly electrical conductor (PEC) walls (Figure 1) is a canonical structure for the comparisons of rectangular and cylindrical FDTD packages, since.

i. Analytical exact (reference) solution can be derived in terms of Green's functions in cylindrical coordinate system;

ii. The structure fits into the cylindrical FDTD space without any staircase discretization error;

iii. The structure may be represented in the rectangular FDTD space with staircase approximation (and introduces discretization errors); and

iv. The structure may also be represented in the rectangular FDTD space if periodic boundary condition (PBC) is applied at both terminations (without using staircase approach).

Any EM problem (structure) can be represented in a discrete environment within the FDTD computation volume either in rectangular or in cylindrical coordinates as long as the problem specific boundary and initial conditions are adequately modeled and stability/numerical dispersion conditions are satisfied. In this study, discretization and numerical modeling of cylindrical structures such as groove resonators [1], microstrip ring resonators [2], is considered via rectangular and cylindrical Finite Difference Time Domain (FDTD) methods, of which preliminary results are discussed in [3].

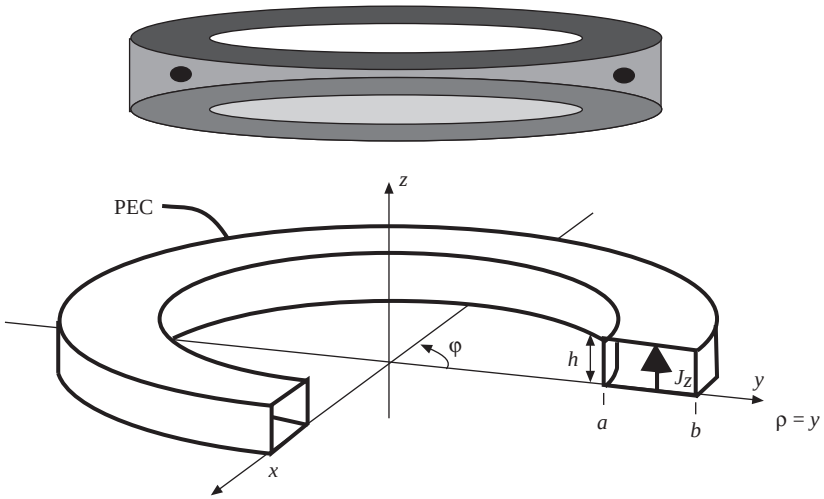

Figure 1. The rectangular ring resonator (top) and its cross-sectional view with illustration of the z-directed excitation (bottom).

2. Ring Resonators and Green's Function Representations

The ring resonator as pictured in Figure 1 is bounded between a and b radially $(a < \rho < b)$, between 0 and h vertically $(0 \le z \le h)$, and between 0 and 2π azimuthally $(0 \le \varphi \le 2\pi)$, where the width w of the cross-section of the ring resonator is $w = b - a$ and the mean peripheral length is $L = \pi(b + a)$. The Green's function problem for a z-directed short dipole source at (ρ', φ', z') inside the resonator can be obtained via the wave equation in the cylindrical coordinate system

$$\left[\frac{1}{\rho}\frac{\partial}{\partial\rho}\left(\rho\frac{\partial}{\partial\rho}\right) + \frac{1}{\rho^2}\frac{\partial^2}{\partial\varphi^2} + \frac{\partial^2}{\partial z^2} + k^2\right] G(\rho, \varphi, z; \rho', \varphi', z') = - \quad \frac{\delta(\rho - \rho')\delta(\varphi - \varphi')\delta(z - z')}{\rho} \tag{1}$$

together with the boundary conditions

$\partial G/\partial z = 0 \text{at } z = 0, h \text{and } G = 0 \text{ at } \rho = a, b$ (1a)

and periodicity condition in φ-direction, where $k$is the free space wavenumber.

The wave equation (1) for the non-penetrable ring resonator can be reduced to three one-dimensional wave equations using the *separation of variables* technique and can be solved separately. Following this procedure yields the solution in terms of first and second kind Bessel functions as [4]

$$\begin{aligned} G(\rho, \varphi, z; \rho', \varphi', z') = & \sum_{m=0}^{\infty} A_m \cos\left(\tfrac{m\pi}{h} z\right) \cos\left(\tfrac{m\pi}{h} z'\right) \\ & \tfrac{1}{2\pi} \sum_{n=-\infty}^{\infty} e^{jn(\varphi - \varphi')} \sum_{l=1}^{\infty} \tfrac{R(\lambda_{mnl}\rho) R(\lambda_{mnl}\rho')}{k^2 - (m\pi/h)^2 - \lambda_{nml}^2} \end{aligned} \tag{2}$$

where

$$A_m = \begin{cases} 1/h & m = 0 \\ 2/h & else \end{cases} \tag{2a}$$

$$R(\lambda\rho) = N\left[J_n(\lambda\rho) + C_1 Y_n(\lambda\rho)\right] \, , C_1 = \frac{J_n(\lambda a)}{Y_n^(\lambda a)} \tag{2b}$$

$$J_n(\lambda b) + \frac{J_n(\lambda a)}{Y_n(\lambda a)} Y_n(\lambda b) = 0 \, at \, \lambda = \lambda_{mnl}, \tag{2c}$$

and the normalization constant is found as

$$N = \frac{1}{\left[\int_a^b \left[R(\lambda_{mnl}\rho)\right] \rho d\rho\right]^{1/2}}. \tag{2d}$$

Here, $J_n(\lambda\rho)$ and $Y_n(\lambda\rho)$are the first and second kind Bessel functions, respectively, and λ_{mnl} correspond to the eigenvalues. Equation (2) can be used to calculate field distribution at any point inside the ring resonator excited by the z-directed short dipole. The resonance frequencies can also be found via the relation

$$f_{mnl} = \frac{c}{2\pi\sqrt{\varepsilon_r}} \sqrt{\left(\frac{m\pi}{h}\right)^2 + \lambda_{mnl}^2}, \tag{3}$$

where ε_r is the relative dielectric permittivity inside homogeneously filled resonator; c denotes the velocity of light. Unfortunately, this requires a triple series summation with infinite number of terms; therefore one need to introduce simplifications in order to reduce the numerical burden. Also, a small loss should be introduced to the medium inside the resonator (i.e., k is assumed complex) in order to avoid numerical problems at frequencies close to the resonator's resonances. A z-directed line source with amplitude I_0 (see Figure 1), i.e.

$$\vec{J}_z = \vec{e}_z I_0 \frac{\delta(\rho - \rho')\delta(\varphi - \varphi')}{\rho}, \tag{4}$$

further simplifies the solution (i.e., $\partial/\partial z \equiv 0$), and triple summation reduces to a double summation. In this case the resonance frequencies are obtained as

$$f_{0nl} = \frac{c}{2\pi\sqrt{\varepsilon_r}} \lambda_{0nl} \tag{5}$$

3. Ring Resonators and FDTD Modeling

Three techniques are used for the FDTD-based numerical analysis of ring resonators together with tests and comparisons among them, as well as against analytical exact solution. The modeling of any type of ring resonators (i.e. groove, microstrip, etc.) via FDTD in both Cartesian and cylindrical coordinates is straightforward. In general, it may be extremely time consuming to work with cylindrical FDTD simulations in the vicinity of the origin ($\rho \to 0$) since the cell size in φ-direction decreases with decreasingρ, and this requires very small time steps in order to satisfy Courant stability criterion. This difficulty is removed if the origin is excluded, as in the ring resonator, or if there is no variation in φ-direction, for example, as in body of revolution (BOR) type radiation problems.

It is possible to model a ring resonator by applying PBC at the both ports of a regular waveguide in Cartesian coordinates to simulate the angular periodicity (Figure 2). Here, the ring resonator given in Figure 1 is also analyzed using rectangular cross section waveguide with the help of "wrap-around" approach required to apply PBC [5].

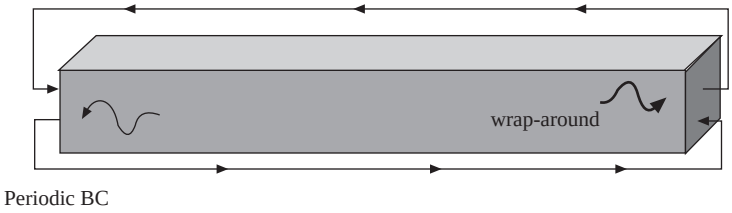

Figure 2. Rectangular cross section waveguide with periodic boundary condition applied at input and output ports.

4. Numerical Applications

Three FDTD packages are prepared for the investigation of ring resonators: R-FDTD based on FDTD in rectangular (Cartesian) coordinates, C-FDTD based on FDTD in cylindrical coordinates and P-FDTD based on rectangular FDTD together with PBC in longitudinal direction. The rectangular system is usually preferred because the spatial cell sizes are uniform over the whole R-FDTD space, while in C-FDTD one side of the cell is $\rho\Delta\varphi$, which varies radially. This should be taken into account when the FDTD parameters are specified.

The validation of the FDTD packages and verification of numerical data are realized via comparisons against analytical exact solution. A circular ring resonator with PEC walls is taken into consideration with parameters $a = 6$ mm, $b = 12$ mm and $h = 1$ mm. The resonator is excited with a z-directed and sine-modulated Gaussian short pulse line source at $\rho' = (a + b)/2$ and $\varphi' = 0$, of which center frequency is 25 GHz and bandwidth is 10 GHz. The cell sizes for C-FDTD and R-FDTD are taken as $\Delta z = \Delta\rho = 0.2$ mm, $\Delta\varphi = 1^\circ$ and $\Delta x = \Delta y = \Delta z = 0.2$ mm, respectively for the first test case. In R-FDTD, the number of cells required to model cylindrical objects is greater, therefore computation time is longer compared to the C-FDTD for the same number of time steps. Here 10,000 time steps is used for the first scenario and E_z is accumulated at an observation point of $\varphi = 120^\circ$, $\rho = (a + b)/2$ and $z = h/2$ for both packages. The resonance frequencies are obtained via off-line discrete Fourier transform (DFT) applied to the recorded $E_z(t)$. The numerical and analytical spectra are plotted in Figure 3. Here, solid and dashed lines, and the symbols correspond to resonance frequencies obtained via R-FDTD, C-FDTD, and the analytic solution, respectively. Since the specified bandwidth does not include resonances corresponding to higher order roots of (2c), only $l = 1$, the first root of (2c), is taken into consideration for the analytical results. Besides, (5) is used to calculate the resonance frequencies since $m = 0$ (i.e., line source in z-axis), therefore in Figure 3 the resonance frequencies 24.85 GHz, 25.43 GHz, 27.11 GHz, 29.67 GHz, 32.89 GHZ, correspond to $n = 0, 1, 2, 3, 4$ with $l = 1$ and $m = 0$, respectively. Although a good agreement between the numerical and analytical results is observed in Figure 3, there is a slight discrepancy between R-FDTD and C-FDTD because of the staircase approximation applied in R-FDTD. This deviation can be reduced if finer cell size (i.e. $\Delta x = \Delta y = \Delta z = 0.1$ mm) is used in R-FDTD. The resonance frequencies obtained via R-FDTD with fine discretization is given in Figure 4 together with C-FDTD and analytical results to emphasize the effect of staircase approach in R-FDTD.

The resonance frequencies are also extracted from the P-FDTD package. In this case, the longitudinal length of the waveguide is chosen to be equal to the mean peripheral of the circular ring resonator $L = \pi(a+b)$. When PBC is applied at the input and output ports of the rectangular cross-section waveguide, the azimuthal periodicity of the circular ring resonator is achieved. The width and height of the rectangular cross-section

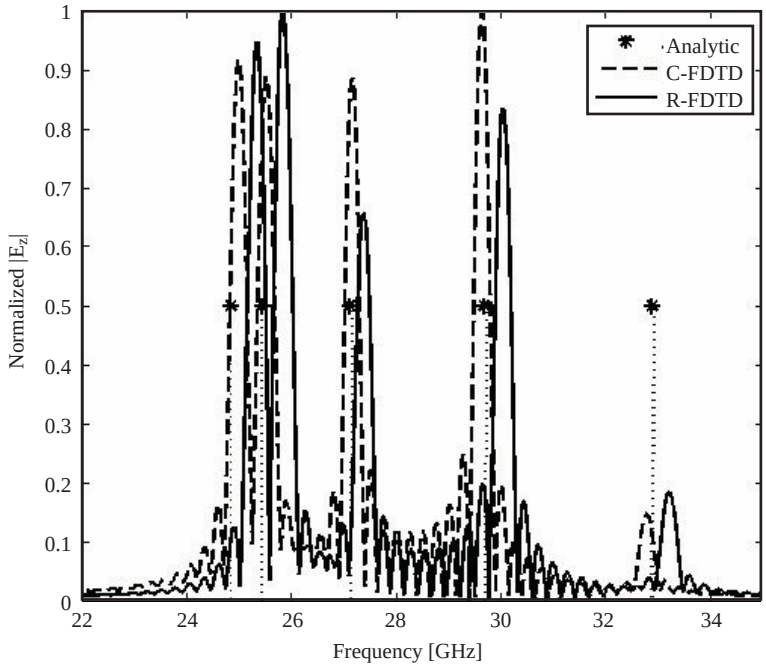

Figure 3. Resonance frequencies obtained via C-FDTD (dashed), R-FDTD with coarse grid (solid) and analytic solution (symbol), where observation point is $\varphi = 120^\circ$, $\rho = (a+b)/2$ and $z = h/2$.

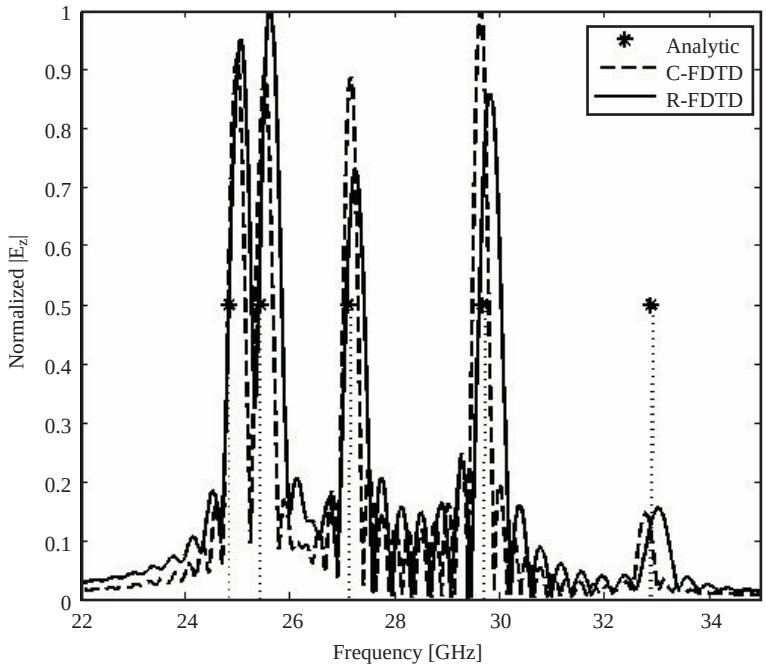

Figure 4. Resonance frequencies obtained via C-FDTD (dashed), R-FDTD with fine grid (solid) and analytic solution (symbol), where observation point is $\varphi = 120^\circ$, $\rho = (a+b)/2$ and $z = h/2$.

waveguide are taken as $w = (b-a)$ and h, respectively. The cell sizes are taken as $\Delta x = \Delta y = \Delta z = 0.2$ mm and the number of cells inside the computation domain is less than the number of cells required in R-FDTD

even for coarse grid case. The resonance frequencies obtained via P-FDTD and C-FDTD are plotted in Figure 5 and Figure 6 for two different observation angles, $\varphi = 120^\circ$ and $\varphi = 90^\circ$, respectively, where

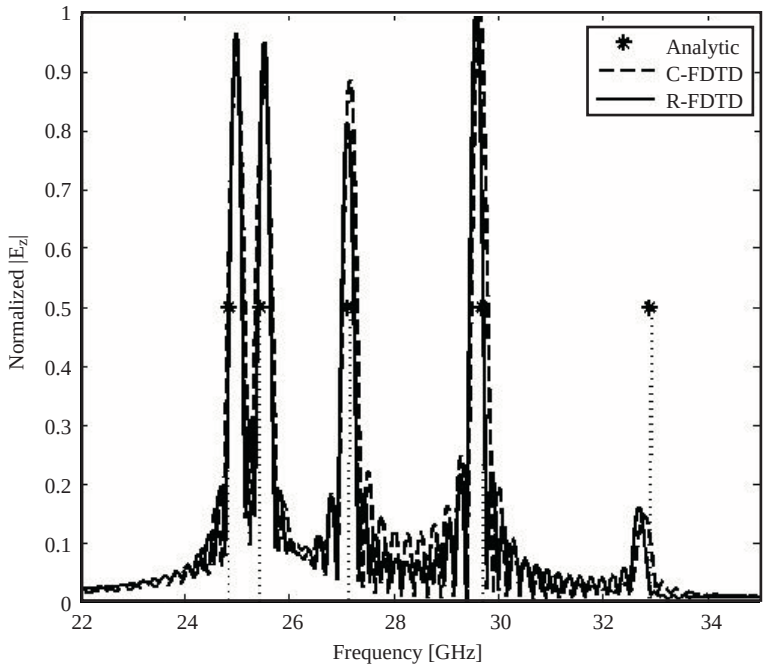

Figure 5. Resonance frequencies obtained via C-FDTD (dashed), P-FDTD (solid) and analytic solution (symbol), where observation point is $\varphi = 120^\circ$, $\rho = (a+b)/2$ and $z = h/2$.

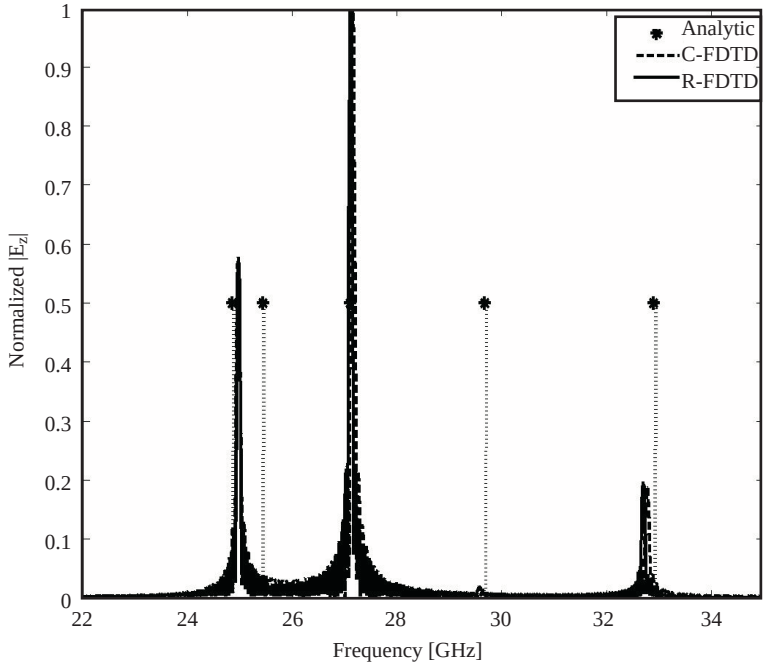

Figure 6. Resonance frequencies obtained via C-FDTD (dashed), P-FDTD (solid) and analytic solution (symbol) where observation point is $\varphi = 90^\circ$, $\rho = (a+b)/2$ and $z = h/2$.

$\rho = (a+b)/2$ and $z = h/2$. The analytical exact solution is also included in the figures. It is clearly observed that there is a good agreement between the three approaches in Figure 5, while the resonance frequencies corresponding to $n = 1$ and $n = 3$, obtained via P-FDTD and C-FDTD, are invisible in Figure 6 compared to the analytical results. This is caused by the fact that the chosen observation angle $\varphi = 90°$ is at the nulls of the related modes since the source angle is at $\varphi = 0°$ (i.e., the modes of these resonances are excited but can not be observed when the observer stands on the modal null points).

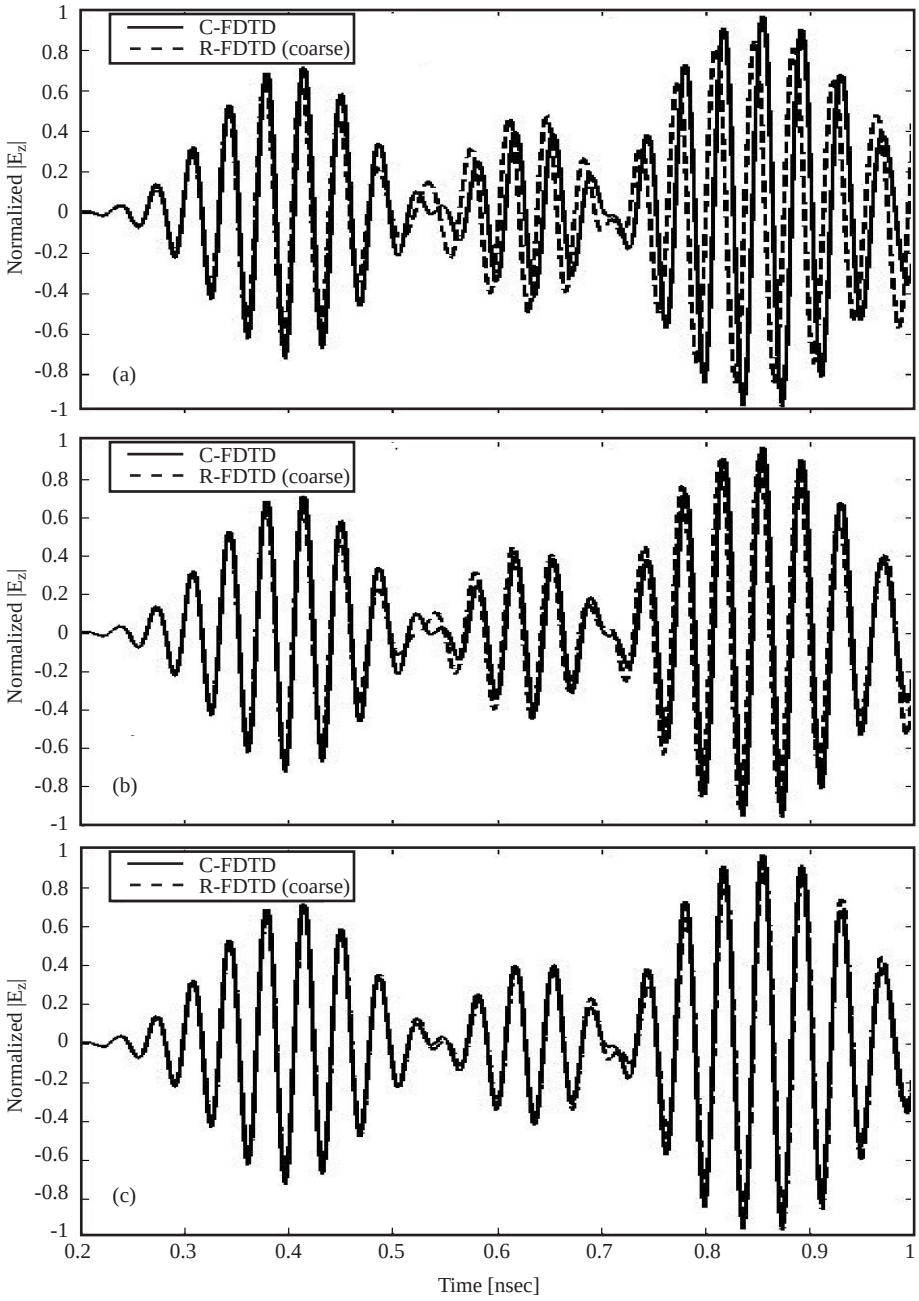

Figure 7. Time variation of normalized $|E_z|$ obtained via C-FDTD (solid) and (a) R-FDTD with coarse mesh (dashed), (b) R-FDTD with fine mesh (dashed) and (c) P-FDTD (dashed).

The last example belongs to the time variation of normalized $|E_z|$ calculated via R-FDTD, P-FDTD and C-FDTD. The results are shown in Figure 7. R-FDTD results obtained with coarse mesh and fine mesh are plotted in Figure 7(a) and 7(b), respectively, in order to show the reformative effect of using finer mesh sizes. Nevertheless, a better agreement is observed in Figure 7(c) between the time domain signatures obtained via P-FDTD and C-FDTD since there is no discretization error in the P-FDTD.

5. Conclusions

Rectangular and cylindrical representations of FDTD method are discussed and compared using a ring (circular) resonator. In-house prepared FDTD codes in rectangular and cylindrical coordinates are used for this purpose. Characteristic tests are performed in both time and frequency domains. The packages are validated against analytical exact solutions derived in cylindrical coordinates. It has also been shown that, the resonance frequencies of a ring resonator can also be obtained using PBC and wrap-around technique at the input and output ports of a finite-length rectangular waveguide. It should be noted that the computation domain is reduced if FDTD with PBC is used instead of R-FDTD in modeling of circular resonator type structures.

References

[1] S. Aydınlık Bechteler, L. Sevgi, "Millimeter waveband semi-symmetrical groove guide resonator", IEEE Microwave Magazine, Vol. 5, No. 3, pp.51-60, Sep 2004

[2] E. Semouchkina, W. Cao, M. Lanagan, R. Mittra, W. Yu "Combining FDTD simulations with measurements of microstrip ring resonators for characterization of low- and high-K dielectrics at microwaves", Microwave and Optical Technology Letters, Vol. 29, No. 21-24, Feb. 2001

[3] F. Akleman, L. Sevgi, "Analytical and numerical investigations of ring resonators" , ICEAA07, Torino, Italy, Sep. 17-21, 2007

[4] A. Ishimaru, Electromagnetic Wave Propagation, Radiation and Scattering, Prentice Hall, 1991

[5] P. Harms, R. Mittra, W. Ko, "Implementation of the periodic boundary condition in the finite-difference time-domain algorithm for FSS structures," *IEEE Trans. Antennas Propagat.,* Vol. 42, No. 9, pp. 1317–1324, Sep. 1994